CHEMISTRY
AN ASIAN JOURNAL
ACES
COMMUNICATION

DOI: 10.1002/asia.201301690

Coordination-Driven Hierarchical Assembly of Silver Nanoparticles on MoS_2 Nanosheets for Improved Lithium Storage

Long Pan,[a] Yi-Tao Liu,*[a] Xu-Ming Xie,*[a] and Xiao-Dong Zhu*[b]

Abstract: We report a novel strategy for the hierarchical assembly of Ag nanoparticles (NPs) on MoS_2 nanosheets through coordination by using a multifunctional organic ligand. The presence of Ag NPs on the surface of MoS_2 nanosheets inhibits their agglomeration, thereby providing increased interlayer spacing for easy Li^+ ion intercalation. Such a unique hybrid architecture also ensures sufficient percolation pathways on the whole surface of the MoS_2 nanosheets. Moreover, the high rigidity and low deformability of the Ag NPs effectively preserve the hybrid architecture during the charge–discharge process, which translates into a high cycle stability. A prominent synergistic effect between MoS_2 and Ag is witnessed. When the Ag content is only 5 wt%, the Ag–MoS_2 hybrid delivers a reversible capacity as high as 920 mA h g^{-1} at a current density of 100 mA g^{-1}, making the Ag–MoS_2 hybrid an attractive candidate for next-generation LIBs.

Today when people are celebrating new scientific and technological progress on the one hand, they are facing a dilemma of energy shortage on the other hand. The development of clean and renewable energy sources is therefore more than a good idea—it is a necessity now. Lithium-ion batteries (LIBs) have become the dominant driving force for portable electronics due to their high energy density and long service life.[1] However, the low specific capacity (372 mA h g^{-1}) of graphite—a commercialized anode material at present—limits the application of LIBs in large-scale devices such as electric vehicles. In this sense, alternative anode materials with better electrochemical performances are particularly desirable.

[a] L. Pan, Dr. Y.-T. Liu, Prof. X.-M. Xie
Key Laboratory of Advanced Materials (Ministry of Education)
Department of Chemical Engineering, Tsinghua University
Beijing 100084 (China)
Fax: (+86) 10 62784550
E-mail: liu-yt03@mails.tsinghua.edu.cn
xxm-dce@mail.tsinghua.edu.cn

[b] Prof. X.-D. Zhu
Academy of Fundamental and Interdisciplinary Sciences
Harbin Institute of Technology
Harbin 150080 (China)
E-mail: zxd9863@163.com

Supporting information for this article is available on the WWW under http://dx.doi.org/10.1002/asia.201301690.

MoS_2 is a typical layered compound in which the molybdenum and sulfur atoms are covalently bonded to form layers held together by weak van der Waals forces.[2] This structure allows easy Li^+ ion intercalation according to the reaction $MoS_2 + 4Li^+ + 4e^- \rightarrow Mo + 2Li_2S$, and the theoretical capacity of MoS_2 is as high as 670 mA h g^{-1}.[3] Unfortunately, the cycle stability and rate capability of MoS_2 are far from satisfactory due to the poor intrinsic conductivity of the material. As such, nanometer-scale carbon materials, including carbon nanotubes and reduced graphene oxide (*r*-GO), have recently been employed as conductive additives to improve the electrochemical performance of MoS_2.[4,5] It is worth noting, however, that the conductivity of such nanometer-scale carbon structures depends heavily on their quality, which is affected by the preparation method and is often inadequate and non-uniform. For example, *r*-GO is structurally disordered and its conductivity is thus destroyed to some extent. Moreover, the reported conductivity of *r*-GO varies by up to two orders of magnitude.[6] Such deficiencies inevitably impose adverse effects on the reproducibility and reliability of the *r*-GO–MoS_2 hybrid anodes. In this context, introducing a small fraction of noble metal nanoparticles (NPs), such as silver, as a conductive additive is a fascinating concept to address this inadequacy and improve the lithium storage capacity of MoS_2 by conductivity resilience.[7] To the best of our knowledge, however, there are no reports to date on developing Ag–MoS_2 hybrids as high-performance anode materials for LIBs.

In situ hydrothermal synthesis is a newly adopted approach to decorating MoS_2 with Ag NPs.[8] Basically, a Ag precursor tends to nucleate and crystallize at the defect sites of MoS_2, resulting in the selective deposition of NPs at the edges and the line defects in the basal planes. This method is limited by its harsh experimental conditions and its inability to control the loading density and distribution of NPs on the nanosheets. The self-assembly of NPs on MoS_2 under mild experimental conditions is thus an elegant alternative to solve these problems.[9] Unfortunately, the chemical inertness of MoS_2 compared to *r*-GO is an obstacle to functionalization by Ag NPs, and a different route is required from the conventional carbon chemistry successfully applied for the Ag–*r*-GO hybrids.[10]

Inspired by the lone pairs on the sulfur surface layers of transition metal disulfides,[11] we have studied the coordination ability of MoS_2 with Cu^{2+} ions.[5a,12] Herein we report, for the first time, a novel strategy for the ex situ hierarchical

assembly of Ag NPs on bare MoS_2 by using a multifunctional organic ligand. Mercaptosuccinic acid (MSA) is bonded to Ag NPs through the Ag–S covalent linkage as a stabilizer.[13] Its carboxylate group, in turn, is linked to the sulfur atoms of MoS_2 through mutual coordination to Cu^{2+} ions. The presence of Ag NPs on the surface of MoS_2 nanosheets inhibits agglomeration, thereby providing increased interlayer spacing for easy Li^+ ion intercalation. Such a unique hybrid architecture also ensures sufficient percolation pathways on the whole surface of MoS_2 nanosheets. The outstanding intrinsic conductivity of Ag NPs facilitates efficient electron transport at a very low content. Last but not least, the high rigidity and low deformability of Ag NPs compared to carbon effectively preserve the hybrid architecture during the charge–discharge process, which translates into a high cycle stability.[7b] A prominent synergistic effect between MoS_2 and Ag is witnessed. When the Ag content is only 5 wt%, the Ag–MoS_2 hybrid delivers a reversible capacity as high as 920 mA h g^{-1}@100 mA g^{-1}. This value may rank the Ag–MoS_2 hybrid as a superior anode candidate for next-generation LIBs. Moreover, the expense of using a small fraction of Ag NPs is justified by this significant performance improvement.

The successful covalent linkage between Ag and the thiol groups of MSA is confirmed by Fourier transform (FT) IR spectroscopy, as shown in Figure 1a. A comparison between the two spectra clearly reveals the formation of Ag–S bonds, since the peak at 2547 cm^{-1} characteristic of S–H stretching vibration disappears after the reaction between MSA and Ag NPs. Moreover, the occurrence of double peaks at 1563 and 1389 cm^{-1} corresponding to C(O)=O asymmetric and symmetric vibration indicates that MSA exists primarily in the form of a carboxylic salt.[13a] The Ag–MSA NPs are readily dispersible in *N*-methyl-2-pyrrolidone (NMP). Detailed observation of the NP morphology and size distribution is realized by AFM and TEM (Figure 1b,c). Generally, the Ag–MSA NPs are homogeneously dispersed in NMP with few, if any, agglomerates. Statistics show that the NPs have a narrow size distribution centered at 8± 1.5 nm (76.5%, inset Figure 1c), which is a huge advantage over the in situ hydrothermally synthesized NPs that are often irregular in both morphology and size.[8] The high-resolution (HR) TEM image (Figure 1d) focusing on an individual Ag–MSA NP reveals a highly crystalline nature with a lattice fringe spacing of approximately 0.23 nm, corresponding to the (111) plane of face-centered cubic (fcc) Ag.[10]

Figure 2 shows schematically the hierarchical assembly of Ag–MSA NPs on MoS_2 by means of coordination as well as the related experimental results. The MoS_2 powder (Figure 2a) can be directly exfoliated in NMP under sonication, producing a dark green solution (Figure 2b) containing MoS_2 nanosheets. Figure 2c shows the TEM image of a large MoS_2 nanosheet with a lateral size of approximately 1.5 μm. HRTEM characterization (Figure 2d) on the edge of a three-layer nanosheet identifies an interlayer spacing of approximately 0.65 nm, which is consistent with the value reported for MoS_2.[2] The atomically resolved HRTEM image (Figure 2e) discloses a perfect hexagonal symmetry of MoS_2 with a lattice constant of approximately 3.2 Å.[14]

The surface sulfur atoms of MoS_2 provide a basis for the coordination-driven hierarchical assembly of Ag–MSA NPs by Cu^{2+} ions. It is found, interestingly, that when the Ag–MSA NPs are absent, the MoS_2 nanosheets agglomerate randomly and thus precipitate from NMP due to their direct cross-linking by Cu^{2+} ions (Figure S6 in the Supporting Information). We also observed similar phenomena on other 2D materials.[15] A small fraction (5 wt%) of Ag–MSA NPs anchored to the MoS_2 nanosheets can effectively prevent their agglomeration by acting as a spacer (Figure 2f–h). The Ag–MSA NPs are uniformly distributed on the MoS_2

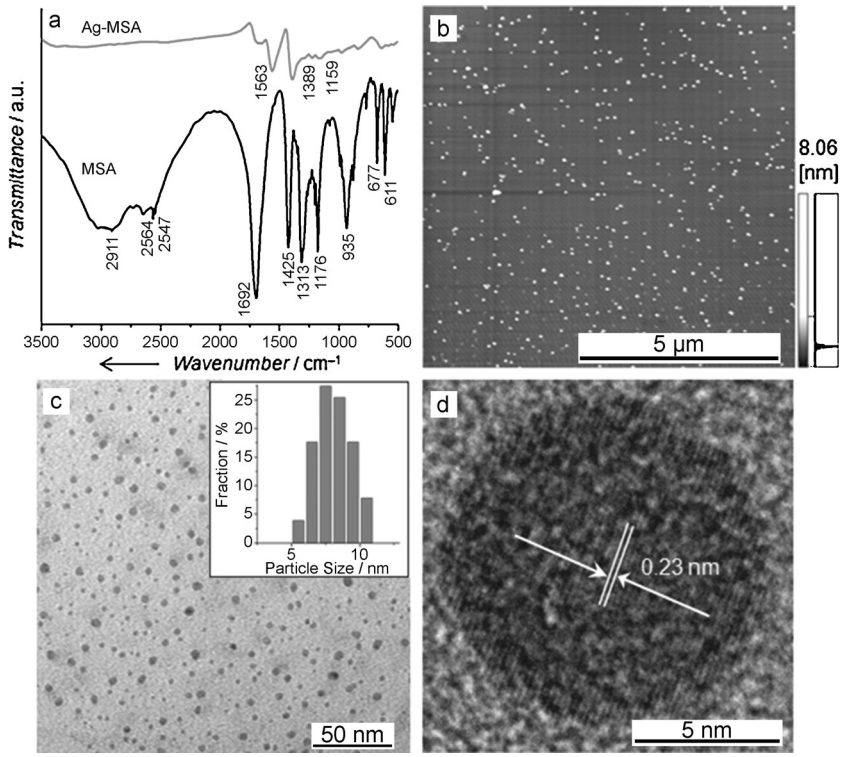

Figure 1. a) FTIR spectra of MSA and Ag–MSA NPs; b) AFM and c) TEM images of Ag–MSA NPs uniformly dispersed in NMP; d) HRTEM image of an individual Ag–MSA NP. The inset in (c) shows a histogram of the Ag NP size distribution.

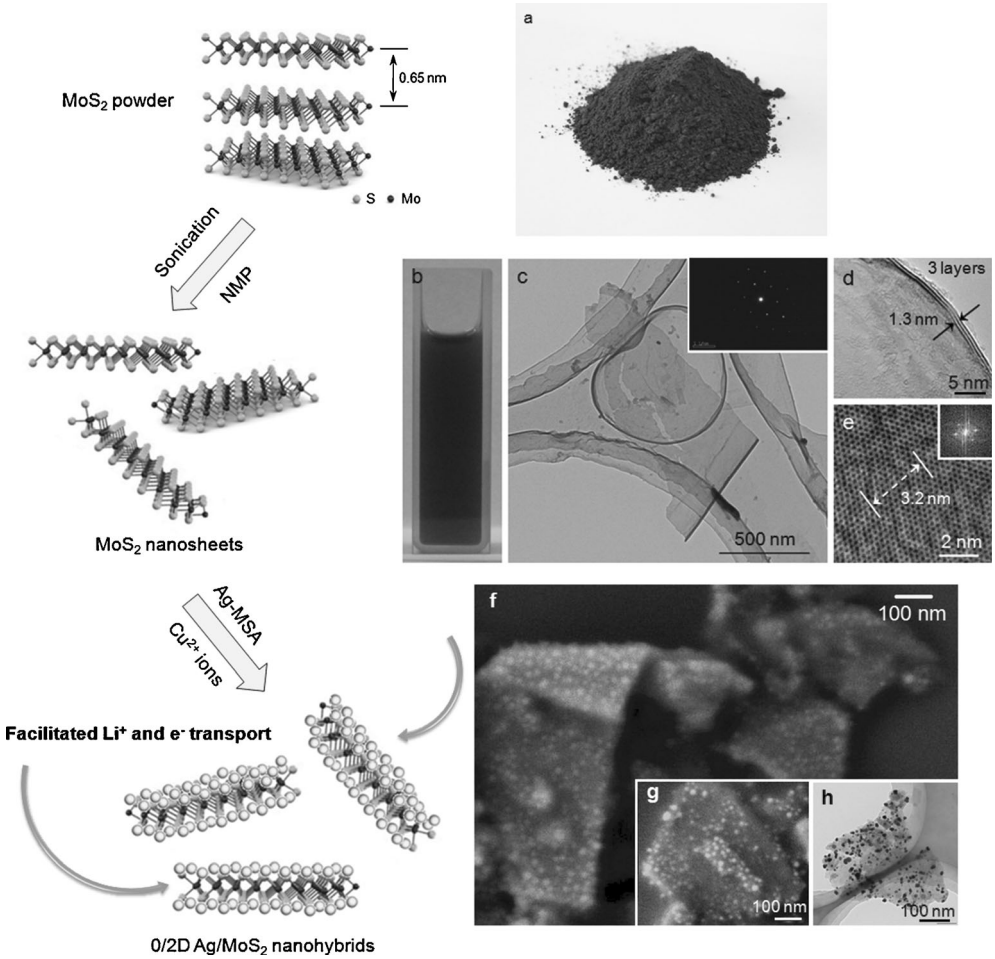

Figure 2. a) Photograph of MoS_2 powder; b) photograph of a MoS_2/NMP solution; c) TEM image of a large MoS_2 nanosheet and the corresponding electron diffraction (ED) pattern (inset); d) HRTEM image of a three-layer MoS_2 nanosheet; e) atomically resolved HRTEM image and the corresponding fast Fourier transform (FFT) image (inset); f, g) SEM and h) TEM images of 5 wt% Ag–MoS_2 hybrid.

surface without an obvious affinity difference. In the HRTEM image (Figure S7 in the Supporting Information), the ripples of the underlying MoS_2 nanosheet supporting the Ag–MSA NPs can easily be recognized. It should be stressed that our strategy can arbitrarily tune the NP loading density on the nanosheets by varying the Ag/MoS_2 ratio (Figure S8 in the Supporting Information). When the Ag content is increased to 15 wt%, a complete coverage of the MoS_2 surface can be seen. In view of the structural integrity of MoS_2 nanosheets (Figure 2e), we infer that the Ag–MSA NPs are likely to be bound to the whole close-packed sulfur surface layers rather than to the defect sites only.[16] It is worth mentioning that even when the Ag–MSA NPs are densely loaded, the MoS_2 nanosheets are still very flexible and can roll up to form "nanotubes" (Figure S9 in the Supporting Information), which is plausible for stress buffering during the subsequent charge–discharge process.

The successful coordination of MoS_2 nanosheets and Ag NPs to Cu^{2+} ions is confirmed by X-ray photoelectron spectroscopy (XPS) characterization (Figure 3). As discussed in the Supporting Information (Figure S4), the C1s XPS spectrum before coordination consists of three types of carbon

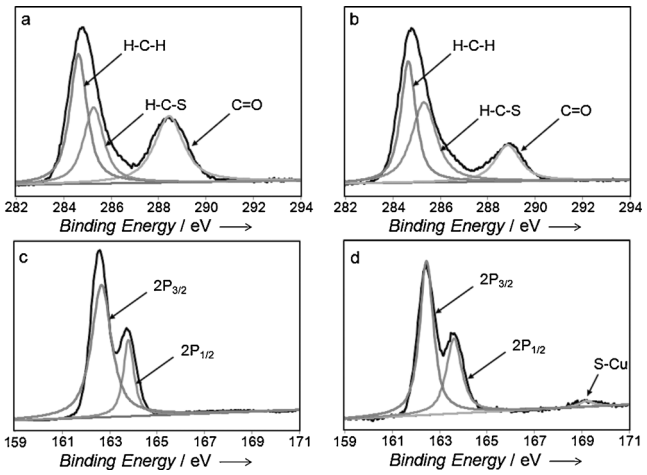

Figure 3. a, b) C1s, and c, d) S2p XPS spectra of Ag–MoS_2 hybrid before (a, c) and after (b, d) coordination.

atoms, that is, C=O bond at 288.5 eV, C–H bond connected to S at 285.3 eV and H–C–H bond at 284.6 eV (Figure 3a).[17] In Figure 3b, a decrease of intensity of the signal

arising from carbon atoms in the C=O bond is witnessed, thus indicating the successful coordination between the carboxylate groups of MSA and Cu^{2+} ions.[12] On the other hand, the S2p XPS spectrum before coordination consists of two well-resolved peaks at 163.8 and 162.6 eV (Figure 3c), corresponding to the $2p_{1/2}$ and $2p_{3/2}$ orbitals of S^{2-}, respectively.[18] After coordination a satellite at 169.2 eV evolves (Figure 3d), demonstrating the formation of a Cu–S complex.[19]

The first two charge–discharge profiles of 5 wt% Ag–MoS_2 hybrid are presented in Figure 4a. The two plateaus at approximately 1.05 and 0.50 V during the first discharge process represent the formation of Li_xMoS_2 and its decomposition into Mo NPs (embedded in a Li_2S matrix), respectively. The slope below approximately 0.50 V is attributed to the generation of a solid-electrolyte interface (SEI) layer originating from electrolyte degradation. During the subsequent sweep a new, inconspicuous plateau at approximately 1.90 V occurs, which is related to the reaction of $Mo+4Li^+ +2S+4e^- \rightarrow 2Li_2S+Mo$ (Mo is left to emphasize its inertness). During the first charge process there is a plateau at approximately 2.25 V. In principle, the polarization between discharge and charge for the conversion of transition metal oxides or sulfides is about 1.0 or 0.6 V.[20,21] However, the actual polarization between discharge and charge of 5 wt% Ag–MoS_2 hybrid is about 1.75 V, which is too high for the oxidation of Mo NPs to MoS_2. Therefore, the plateau at approximately 2.25 V is ascribed to the conversion of Li_2S to S, and it stays unchanged during the subsequent sweep.[3e] These results are in good agreement with the cyclic voltammetry curves (Figure 4b).

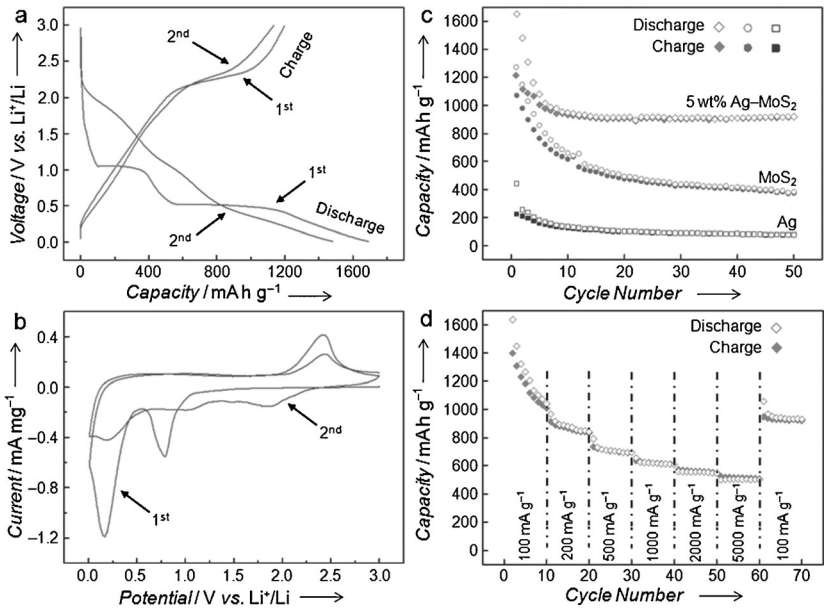

Figure 4. a) Charge–discharge (current density 100 mA g^{-1}) and b) cyclic voltammetry (scan rate 0.1 mV s^{-1}) curves of 5 wt% Ag–MoS_2 hybrid; c) cycle behaviors (current density 100 mA g^{-1}) of Ag–MSA NPs, neat MoS_2, and 5 wt% Ag–MoS_2 hybrid; d) rate capability of 5 wt% Ag–MoS_2 hybrid.

Figure 4c displays the cycle behaviors of Ag–MSA NPs, MoS_2, and 5 wt% Ag–MoS_2 hybrid. Neat MoS_2 has an initial discharge capacity of 1275 mA h g^{-1}, a value much higher than its theoretical capacity due to the increased interlayer spacing arising from the liquid-phase exfoliation. Unfortunately, the low conductivity and pulverization problem of MoS_2 leads to rapid capacity fading to 382 mA h g^{-1} at the 50th cycle. However, when only 5 wt% Ag–MSA NPs are introduced, an extraordinarily high cycle stability is witnessed with a reversible capacity up to 920 mA h g^{-1} after 50 cycles, which can rival or even outperform the achievement reported for carbonaceous additives at a much higher loading.[4,5] Moreover, the 5 wt% Ag–MoS_2 hybrid exhibits an excellent rate capability when cycled at a higher current density. The reversible capacity remains at 840 or 695 mA h g^{-1} for current densities of 200 or 500 mA g^{-1} and is still above 500 mA h g^{-1} when the current density is as high as 5000 mA g^{-1}, emphasizing a prominent synergistic effect between MoS_2 and Ag. When the current density is recovered to 100 mA g^{-1}, the reversible capacity returns to 930 mA h g^{-1} immediately, once again demonstrating the high cycle stability of the Ag–MoS_2 hybrid. The expense of using a small fraction of Ag is thus justified by this significant performance improvement. Here Ag plays three important roles: 1) as a high-efficiency conductive additive to increase the conductivity of the Ag–MoS_2 hybrid; 2) as an interlayer spacer to prevent the agglomeration of MoS_2 nanosheets and allow for easy Li^+ ion intercalation; 3) as a rigid structural strengthener to preserve the Ag–MoS_2 hybrid architecture during the charge–discharge process. It is worth mentioning, however, that the increased interlayer spacing in the Ag–MoS_2 hybrid means more Li^+ ions may be trapped in the surface voids and defects of the active material, resulting in a relatively low Coulombic efficiency during the first five cycles. Note that although Ag can alloy with Li,[22] its extremely low capacity (Figure 4c) determines that the Ag–MSA NPs mainly serve as a conductive additive and contribute little to the measured capacity, which is in accord with a previous report.[7b]

In summary, we have developed a novel strategy for the hierarchical assembly of Ag NPs on MoS_2 through coordination. The strong interaction between Ag NPs and MoS_2 facilitated by coordination inhibits their separation during the charge–discharge process, which is advantageous over other

weak interactions, such as van der Waals forces. The introduction of Ag NPs ensures efficient electron transport at a very low content. Moreover, their high rigidity and low deformability effectively strengthen the hybrid architecture. The Ag–MoS_2 hybrid exhibits a significantly improved lithium storage capacity, thus holding great promise in next-generation LIBs.

Experimental Section

The synthesis of Ag–MSA NPs was adapted from the literature.[13] In a typical experiment, $AgNO_3$ (10 mmol, 1.70 g) and MSA (10 mmol, 1.50 g) were dissolved in deionized water (100 mL) under stirring. Fresh $NaBH_4$ (20 mmol, 0.76 g) in water (20 mL) was added dropwise to the as-prepared solution over a period of 10 min. The mixed solution was stirred at ambient temperature for 2 h to achieve a complete reaction. A mixture of deionized water and acetone was then added to the solution to precipitate the Ag–MSA NPs, which were separated by high-speed centrifugation at 11000 rpm for 20 min and washed by a mixture of deionized water and acetone three times. After being washed the Ag–MSA NPs were dried in a vacuum oven at 30 °C. The procedures for exfoliating the MoS_2 powder in NMP were adapted from a previous report.[23] Briefly, the MoS_2 powder was added to NMP at an initial concentration of 10 mg mL^{-1}, homogenized at 11500 rpm for 60 min, and then subjected to sonication at 300 W for 60 min. The obtained slurry was centrifuged at 1500 rpm for 45 min, and the top half of the supernatant was collected. The collected supernatant was further centrifuged at 3000 rpm for another 45 min. The precipitated solid was collected and re-dispersed in NMP by sonication, yielding a dark green MoS_2/NMP solution containing relatively large MoS_2 nanosheets. The Ag–MSA NPs were mixed with the exfoliated MoS_2 nanosheets in NMP at different ratios, followed by the addition of dehydrated $CuCl_2$ at a MoS_2/Cu^{2+} molar ratio of 10:1 The mixed solution was kept under gentle sonication (60 W) for 48 h to ensure an adequate reaction while preventing the precipitation of MoS_2 nanosheets. Next, the mixed solution was centrifuged at 11000 rpm for 60 min to collect the Ag–MoS_2 hybrids, which were washed by deionized water repeatedly. It was found that when the Ag content was below 15 wt%, the Ag–MSA NPs could be completely assembled on the MoS_2 nanosheets. After centrifugation, there were few, if any, free Ag–MSA NPs left in the NMP solution (as confirmed by TEM observation). Moreover, the solution after centrifugation was nearly transparent and colorless, further demonstrating that the Ag–MSA NPs were completely assembled on the MoS_2 nanosheets. An anode was prepared by coating a copper foil (current collector) with a slurry containing 80 wt% active material, 10 wt% acetylene black and 10 wt% poly(vinylidene fluoride) dissolved in NMP. The anode was then dried in nitrogen at 120 °C for 12 h to adequately evaporate the residual organic solvent and equipped in a half cell according to the configuration of (−) Li | electrolyte | anode (+) with a liquid electrolyte (1 M solution of $LiPF_6$ in ethylene carbonate/dimethyl carbonate at a volume ratio of 1:1) in a vacuum glove box. A microporous polypropylene membrane was used as the separator. The active material was Ag–MSA NPs, neat MoS_2, or 5 wt% Ag–MoS_2 hybrid.

Acknowledgements

We sincerely thank the National Natural Science Foundation of China (Nos. 21304053, 21274079 and 21246011) and the Specialized Research Fund for the Doctoral Program of Higher Education (Nos. 20110002110032 and 20120002130012) for financial support. Y.-T.L. acknowledges the China Postdoctoral Science Foundation (No. 2013M530616).

Keywords: hybrid architectures · layered compounds · lithium-ion batteries · molybdenum · silver

[1] a) H. Guan, X. Wang, H. Li, C. Zhi, T. Zhai, Y. Bando, D. Golberg, *Chem. Commun.* **2012**, *48*, 4878–4880; b) S. Sen, K. Moses, A. J. Bhattacharyya, C. N. R. Rao, *Chem. Asian J.* **2014**, *9*, 100–103; c) X.-L. Wu, Y.-G. Guo, L.-J. Wan, *Chem. Asian J.* **2013**, *8*, 1948–1958; d) X. Huang, B. Sun, S. Chen, G. Wang, *Chem. Asian J.* **2014**, *9*, 206–211; e) Y. Wang, G. Wang, *Chem. Asian J.* **2013**, *8*, 3142–3146; f) H. Wang, D. Ma, X. Huang, Y, Huang, X. Zhang, *Sci. Rep.* **2012**, *2*, 701; g) X. Huang, R. Wang, D. Xu, Z. Wang, H. Wang, J. Xu, Z. Wu, Q. Liu, Y. Zhang, X. Zhang, *Adv. Funct. Mater.* **2013**, *23*, 4345–4353; h) Z. Wang, D. Xu, Y. Huang, Z. Wu, L. Wang, X. Zhang, *Chem. Commun.* **2012**, *48*, 976–978.

[2] H. S. S. Ramakrishna Matte, A. Gomathi, A. K. Manna, D. J. Late, R. Datta, S. K. Pati, C. N. R. Rao, *Angew. Chem.* **2010**, *122*, 4153–4156; *Angew. Chem. Int. Ed.* **2010**, *49*, 4059–4062.

[3] a) G. Du, Z. Guo, S. Wang, R. Zeng, Z. Chen, H. Liu, *Chem. Commun.* **2010**, *46*, 1106–1108; b) S. Ding, D. Zhang, J. S. Chen, X. W. Lou, *Nanoscale* **2012**, *4*, 95–98; c) X. Fang, C. Hua, X. Guo, Y. Hu, Z. Wang, X. Gao, F. Wu, J. Wang, L. Chen, *Electrochim. Acta* **2012**, *81*, 155–160; d) X. Fang, X. Guo, Y. Mao, C. Hua, L. Shen, Y. Hu, Z. Wang, F. Wu, L. Chen, *Chem. Asian J.* **2012**, *7*, 1013–1017; e) X. Fang, X. Yu, S. Liao, Y. Shi, Y.-S. Hu, Z. Wang, G. D. Stucky, L. Chen, *Microporous Mesoporous Mater.* **2012**, *151*, 418–423.

[4] a) K. Bindumadhavan, S. K. Srivastava, S. Mahanty, *Chem. Commun.* **2013**, *49*, 1823–1825; b) S.-Y. Tai, C.-J. Liu, S.-W. Chou, F. S.-S. Chien, J.-Y. Lin, T.-W. Lin, *J. Mater. Chem.* **2012**, *22*, 24753–24759; c) S.-K. Park, S.-H. Yu, S. Woo, B. Quan, D.-C. Lee, M. K. Kim, Y.-E. Sung, Y. Piao, *Dalton Trans.* **2013**, *42*, 2399–2405; d) S. Ding, J. S. Chen, X. W. Lou, *Chem. Eur. J.* **2011**, *17*, 13142–13145; e) J.-Z. Wang, L. Lu, M. Lotya, J. N. Coleman, S.-L. Chou, H.-K. Liu, A. I. Minett, J. Chen, *Adv. Energy Mater.* **2013**, *3*, 798–805.

[5] a) Y.-T. Liu, X.-D. Zhu, Z.-Q. Duan, X.-M. Xie, *Chem. Commun.* **2013**, *49*, 10305–10307; b) X. Zhou, L.-J. Wan, Y.-G. Guo, *Chem. Commun.* **2013**, *49*, 1838–1840; c) K. Chang, W. Chen, *Chem. Commun.* **2011**, *47*, 4252–4254; d) K. Chang, W. Chen, *ACS Nano* **2011**, *5*, 4720–4728; e) G. Huang, T. Chen, W. Chen, Z. Wang, K. Chang, L. Ma, F. Huang, D. Chen, J. Y. Lee, *Small* **2013**, *9*, 3693–3703; f) H. Yu, C. Ma, B. Ge, Y. Chen, Z. Xu, C. Zhu, C. Li, Q. Ouyang, P. Gao, J. Li, C. Sun, L. Qi, Y. Wang, F. Li, *Chem. Eur. J.* **2013**, *19*, 5818–5823.

[6] O. C. Compton, S. T. Nguyen, *Small* **2010**, *6*, 711–723.

[7] a) Y. Yu, L. Gu, C. Zhu, S. Tsukimoto, P. A. van Aken, J. Maier, *Adv. Mater.* **2010**, *22*, 2247–2250; b) D. Chen, X. Mei, G. Ji, M. Lu, J. Xie, J. Lu, J. Y. Lee, *Angew. Chem.* **2012**, *124*, 2459–2463; *Angew. Chem. Int. Ed.* **2012**, *51*, 2409–2413; c) S. H. Nam, H.-S. Shim, Y.-S. Kim, M. A. Dar, J. G. Kim, W. B. Kim, *ACS Appl. Mater. Interfaces* **2010**, *2*, 2046–2052; d) H. Cheng, Z. G. Lu, J. Q. Deng, C. Y. Chung, K. Zhang, Y. Y. Li, *Nano Res.* **2010**, *3*, 895–901; e) D. Guan, Y. Wang, *Ionics* **2013**, *19*, 879–885; f) X. Yang, Z. Wen, S. Huang, X. Zhu, X. Zhang, *Solid State Ionics* **2006**, *177*, 2807–2810.

[8] a) X. Huang, Z. Zeng, S. Bao, M. Wang, X. Qi, Z. Fan, H. Zhang, *Nat. Commun.* **2013**, *4*, 1444; b) B. G. Rao, H. S. S. Ramakrishna Matte, C. N. R. Rao, *J. Cluster Sci.* **2012**, *23*, 929–937.

[9] Y.-T. Liu, Z.-Q. Duan, X.-M. Xie, X.-Y. Ye, *Chem. Commun.* **2013**, *49*, 1642–1644.

[10] a) X.-Z. Tang, Z. Cao, H.-B. Zhang, J. Liu, Z.-Z. Yu, *Chem. Commun.* **2011**, *47*, 3084–3086; b) Z. Zhang, F. Xu, W. Yang, M. Guo, X. Wang, B. Zhang, J. Tang, *Chem. Commun.* **2011**, *47*, 6440–6442; c) X. Lu, H. Qi, X. Zhang, Z. Xue, J. Jin, X. Zhou, X. Liu, *Chem. Commun.* **2011**, *47*, 12494–12496; d) C. Xu, X. Wang, *Small* **2009**, *5*, 2212–2217.

[11] a) M. N. Tahir, N. Zink, M. Eberhardt, H. A. Therese, U. Kolb, P. Theato, W. Tremel, *Angew. Chem.* **2006**, *118*, 4927–4933; *Angew. Chem. Int. Ed.* **2006**, *45*, 4809–4815; b) M. N. Tahir, N. Zink, M.

Eberhardt, H. A. Therese, S. Faiss, A. Janshoff, U. Kolb, P. Theato, W. Tremel, *Small* **2007**, *3*, 829–834.
[12] Y.-T. Liu, Z. Tan, X.-M. Xie, Z.-F. Wang, X.-Y. Ye, *Chem. Asian J.* **2013**, *8*, 817–823.
[13] a) L. Qi, B. I. Lee, S. Chen, W. D. Samuels, G. J. Exarhos, *Adv. Mater.* **2005**, *17*, 1777–1781; b) E. Sumesh, M. S. Bootharaju, A. T. Pradeep, *J. Hazard. Mater.* **2011**, *189*, 450–457.
[14] J. A. Wilson, A. D. Yoffe, *Adv. Phys.* **1969**, *18*, 193–335.
[15] a) Y.-T. Liu, X.-M. Xie, X.-Y. Ye, *Chem. Commun.* **2013**, *49*, 388–390; b) Y.-T. Liu, Q.-P. Feng, X.-M. Xie, X.-Y. Ye, *Carbon* **2011**, *49*, 3371–3375; c) Y.-T. Liu, M. Dang, X.-M. Xie, Z.-F. Wang, X.-Y. Ye, *J. Mater. Chem.* **2011**, *21*, 18723–18729.
[16] C. Shahar, R. Levi, S. R. Cohen, R. Tenne, *J. Phys. Chem. Lett.* **2010**, *1*, 540–543.
[17] T. U. B. Rao, T. Pradeep, *Angew. Chem.* **2010**, *122*, 4017–4021; *Angew. Chem. Int. Ed.* **2010**, *49*, 3925–3929.
[18] K.-K. Liu, W. Zhang, Y.-H. Lee, Y.-C. Lin, M.-T. Chang, C.-Y. Su, C.-S. Chang, H. Li, Y. Shi, H. Zhang, C.-S. Lai, L.-J. Li, *Nano Lett.* **2012**, *12*, 1538–1544.
[19] S. Larsson, *J. Am. Chem. Soc.* **1977**, *99*, 7708–7709.
[20] A. Debart, L. Dupont, R. Patrice, J. M. Tarascon, *Solid State Sci.* **2006**, *8*, 640–651.
[21] Y. Kim, J. B. Goodenough, *J. Phys. Chem. C* **2008**, *112*, 15060–15064.
[22] Y. J. Lee, Y. Lee, D. Oh, T. Chen, G. Ceder, A. M. Belcher, *Nano Lett.* **2010**, *10*, 2433–2440.
[23] J. N. Coleman, M. Lotya, A. O'Neill, S. D. Bergin, P. J. King, U. Khan, K. Young, A. Gaucher, S. De, R. J. Smith, I. V. Shvets, S. K. Arora, G. Stanton, H.-Y. Kim, K. Lee, G. T. Kim, G. S. Duesberg, T. Hallam, J. J. Boland, J. J. Wang, J. F. Donegan, J. C. Grunlan, G. Moriarty, A. Shmeliov, R. J. Nicholls, J. M. Perkins, E. M. Grieveson, K. Theuwissen, D. W. McComb, P. D. Nellist, V. Nicolosi, *Science* **2011**, *331*, 568–571.

Received: December 19, 2013
Revised: January 29, 2014
Published online: March 26, 2014